

# CuFeO<sub>2</sub> at a megabar: Stabilization of a mixed-valence low-spin magnetic semiconducting ground state

W. M. Xu,<sup>1,\*</sup> G. R. Hearne,<sup>2</sup> and M. P. Pasternak<sup>1</sup><sup>1</sup>*School of Physics and Astronomy, Tel Aviv University, Ramat-Aviv 69978, Tel Aviv, Israel*<sup>2</sup>*Department of Physics, University of Johannesburg, P.O. Box 524, Auckland Park, 2006, Johannesburg, South Africa*

(Received 2 June 2016; revised manuscript received 7 July 2016; published 27 July 2016)

The magnetic and electrical-transport properties of CuFeO<sub>2</sub> have been studied by temperature-dependent <sup>57</sup>Fe Mössbauer spectroscopy and resistance measurements to near megabar (~100 GPa) pressures. Previous studies show that CuFeO<sub>2</sub> comprises the following sublattices at  $P > 23$  GPa:  $\frac{1}{3}[\text{Cu}_{(S=1/2)}^{2+}\text{Fe}_{(S=2)}^{2+}\text{O}_2] + \frac{2}{3}[\text{Cu}_{(S=0)}^{1+}\text{Fe}_{(S=5/2)}^{3+}\text{O}_2]$ . The magnetic ordering temperatures of the sublattices, with both Fe valences in the high-spin state, reach a maximum at ~50 GPa. At higher pressures two different magnetic components with collapsed magnetic hyperfine fields of 0 and ~10 T have been detected by the Mössbauer probe. The pressure evolution and temperature dependence of the associated hyperfine interaction parameters to ~95 GPa identifies these as low-spin Fe<sub>(S=0)</sub><sup>2+</sup> and Fe<sub>(S=1/2)</sub><sup>3+</sup> states in the very-high-pressure phase of CuFeO<sub>2</sub>. The Fe<sup>3+</sup> low-spin state exhibits an unusually high onset temperature for magnetic ordering,  $T_M \sim 50$  K. Resistance-temperature dependences show CuFeO<sub>2</sub> in the low-spin state at very high pressure to be a narrow-gap semiconductor with variable range hopping of charge carriers. The derived Mott temperature from this conductivity mechanism,  $T_0$ , undergoes an appreciable decrease from ~50 GPa onwards where the spin-crossover regions nucleate and grow with increasing abundance in the lattice. An extrapolated  $T_0$  value of ~10<sup>5</sup> K at 100 GPa is interpreted as persistent charge carrier confinement in the low-spin phase. At these high densities a mixed-valence low-spin magnetic semiconducting ground state has been stabilized, in which strong electron correlations are persistent.

DOI: [10.1103/PhysRevB.94.035155](https://doi.org/10.1103/PhysRevB.94.035155)

## I. INTRODUCTION

The two-dimensional triangular (“frustrated”) lattice system CuFeO<sub>2</sub>, delafossite, exhibits diverse electronic phase transitions under external high pressure and has been intensively studied in recent years. Its constituent valence states, magnetism and structure, at pressure have been investigated by <sup>57</sup>Fe Mössbauer spectroscopy (MS) [1,2] and x-ray absorption spectroscopy [2], neutron scattering [3,4] and x-ray diffraction [2,5] up to 30 GPa by different groups.

At ambient pressure, the crystal structure of CuFeO<sub>2</sub> belongs to the space group  $R\bar{3}m$  with  $a_h = 3.03$  Å and  $c_h = 17.09$  Å in the hexagonal description [6]. The structure consists of hexagonal layers of Cu<sup>1+</sup>, Fe<sup>3+</sup>, and O<sup>2-</sup> with a stacking sequence of *A-B-C* [*A*(Cu), *A*(O), *B*(Fe), *C*(O), *C*(Cu), *C*(O), *A*(Fe), etc.] along the *c* axis to form layered triangular lattice antiferromagnetism. Triangular sublattices of magnetic Fe<sup>3+</sup> are separated by nonmagnetic sublattice layers of Cu<sup>1+</sup> and O<sup>2-</sup>. Successive magnetic transitions occur at  $T_{N1} = 16$  K to a partially disordered phase and  $T_{N2} = 11$  K to a four-sublattice long-range magnetically ordered system, based on powder neutron diffraction studies [7].

Neutron diffraction measurements show that above ~6 GPa the magnetic ground state of CuFeO<sub>2</sub> is a collinear spin-density wave [4]. Up to 17 GPa, the four-sublattice long-range magnetic order of CuFeO<sub>2</sub> is gradually suppressed and the partially ordered magnetic phase becomes dominant. At ~18 GPa only a single magnetically ordered component could be discerned by <sup>57</sup>Fe MS, with static magnetic ordering onset at  $T_M \sim 40$  K. This coincides with a symmetry change to a more isotropic *C2/c* structure, designated HP1. In the range

24–27 GPa, overlapping of Cu and Fe *3d* bands and associated interlayer Cu<sup>1+</sup> → Fe<sup>3+</sup> electronic charge transfer result in Fe<sup>3+</sup> and Fe<sup>2+</sup> mixed-valence states occurring in a ratio of 2:1 [2]. This electronic transition is related to a structural change in which coexisting domains of *C2/c* and  $P\bar{3}m$  symmetry occur, associated with Fe<sup>3+</sup> and Fe<sup>2+</sup> valences, respectively.

The main aim of the present work is to investigate the pressure response of magnetic-electronic properties of this mixed-valence phase (designated CuFeO<sub>2</sub>-HP2) to well beyond its onset at 24–27 GPa. This has been accomplished by way of an in-house <sup>57</sup>Fe MS probe to near 100 GPa. Concurrent electrical-transport properties of CuFeO<sub>2</sub> are studied by resistance-temperature measurements to ~80 GPa. Such high densities will have important consequences for the Fe *3d* electronic manifold. There is likely to be a substantial increase in the *3d* crystal field splitting for both valences and the relatively large ionic radius involved in the high-spin states, particularly that of Fe<sup>2+</sup>, cannot be accommodated in the compressed lattice. A consequence of this may be high-spin (HS) to low-spin (LS) crossover, “on-site spin pairing,” occurring concurrently for both Fe valences. One of the objectives of this investigation is to check whether this occurs at sufficiently high densities by using a suitable direct probe of the Fe *3d* electronic states. Furthermore we are interested in the impact of this *3d* crystal field evolution on the anticipated Mott transition (breakdown of strong electron correlations) in such a mixed-valence magnetic system.

## II. EXPERIMENT

A polycrystalline sample was prepared by thoroughly grinding and mixing starting oxides Cu<sub>2</sub>O and Fe<sub>2</sub>O<sub>3</sub>, with

\*xuw@post.tau.ac.il

the latter having 20%  $^{57}\text{Fe}$  enrichment. The oxide mixture was pressed into disks and fired at 900 °C for 24 h, after which it was quenched to room temperature, reground, repelleted and refired for a further 24-h period before a final quench to obtain single-phase material [2]. All firing and quenching has been performed in an ambient nitrogen atmosphere.

The Tel Aviv miniature piston-cylinder diamond anvil cell (DAC) was used for pressurization [8]. Diamond anvils had 300- or 250- $\mu\text{m}$  culet diameters for the pressure ranges 2–60 GPa and 60–95 GPa, respectively. Samples were loaded into 150- or 100- $\mu\text{m}$  cavity diameters drilled in a Re gasket that also served as a collimator for the 14.4-keV probing  $\gamma$  radiation. Argon was used as a pressure transmitting medium in the case of the Mössbauer measurements, whereas we relied on the initially soft surrounding insulating medium for transmitting pressure in the resistance studies. The fluorescence from tiny ruby fragments loaded along with the sample served for pressure determination. The error of the pressure measurement is  $\sim 5\%$  of the quoted (average) value.

$^{57}\text{Fe}$  Mössbauer pressure studies were carried out with a  $^{57}\text{Co}(\text{Rh})$  10 mCi point source in the 4.2–300 K temperature range using a top-loading liquid helium cryostat [9]. Source and absorber sample were kept at nearly the same temperature. Typical data collection time of a single spectrum was  $\sim 24$  h to obtain sufficient signal-to-noise ratios for a reliable analysis.

Resistance pressure studies in the 5–300 K range were performed with thin miniature Pt electrodes mounted on one of the culets and overlapped with the edge of the sample. These were insulated from the metal gasket using a mixture of alumina and NaCl. The DAC was mounted in a special holder for vertical adjustment in a commercial liquid helium Dewar. A PC-controlled dc motor ensured that the height of the DAC holder above the liquid helium level could be changed for relatively well controlled heating or cooling in the cold helium exchange gas. Both temperature from a calibrated Si-diode thermometer and resistance of the pressurized sample were recorded simultaneously using four-probe methods. Pressure was determined from the ruby fragment located in the region between the electrode tips, near the center of the sample area.

### III. RESULTS

#### A. $^{57}\text{Fe}$ Mössbauer pressure investigation

Mössbauer spectra of  $\text{CuFeO}_2$  from 27 to 95 GPa at 5 K, representing the pressure evolved magnetic-electronic ground state of the system are depicted in Fig. 1. The full Hamiltonian is used in fitting subcomponents, to cater for cases where the quadrupole interaction is comparable in strength to the magnetic interaction, e.g., cases of high-spin  $\text{Fe}^{2+}$  (atomic spin  $S = 2$ ) and low-spin  $\text{Fe}^{3+}$  ( $S = 1/2$ ). The following spin Hamiltonian, representing the excited ( $I^* = 3/2$ ) and ground ( $I = 1/2$ ) nuclear spin states of the 14.4-keV resonance of  $^{57}\text{Fe}$ , was utilized to fit measured spectra and extract hyperfine interaction parameters indicative of iron valence and  $3d$  spin states [10,11]:

$$H(I^*) = -\mu^* \left( \frac{I_z}{I^*} \right) H_{hf}(\theta) + \frac{e^2 q_{zz} Q}{4I^*(2I^* - 1)} \times [3I_z^2 - I^*(I^* + 1)], \quad (1a)$$

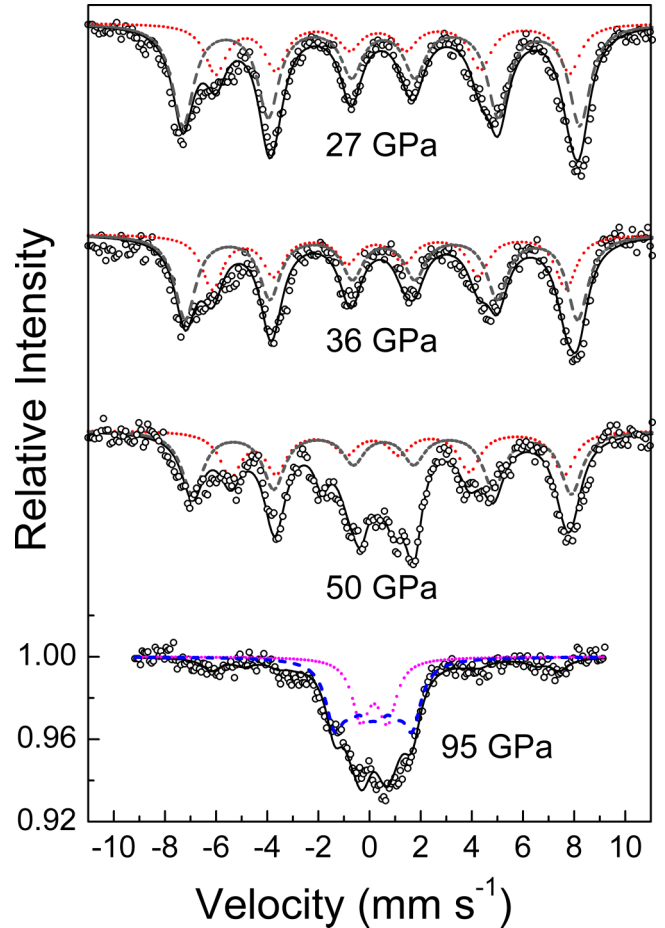


FIG. 1. Mössbauer spectra of  $\text{CuFeO}_2$  from 27 to 95 GPa at 5 K. Open circles are the original experimental data. The solid line through experimental points is the overall theoretical fit. Dashed and dotted lines are subspectra corresponding to  $\text{Fe}^{3+}$  and  $\text{Fe}^{2+}$ , respectively.

and

$$H(I) = -\mu \left( \frac{I_z}{I} \right) H_{hf}. \quad (1b)$$

The ground- and excited-state nuclear moments are  $\mu$  and  $\mu^*$ , respectively. The angle between internal magnetic field  $H_{hf}$  and the maximum value of the electric field gradient (EFG),  $e q_{zz}$ , is  $\theta$ . The quadrupole coupling is  $e^2 q_{zz} Q$  (where  $Q$  is the quadrupole moment), which is part of the quadrupole shift or quadrupole splitting parameters,  $\Delta_{QS}$ , obtained from fitting magnetic sextet or doublet subcomponents, respectively [12]. The asymmetry parameter  $\eta$ , linking all diagonal components of the EFG tensor, is assumed as zero in Eq. 1(a). It can normally only be determined reliably in well resolved high-quality spectra and has minimal influence on other pertinent hyperfine interaction parameters extracted in this study. All isomer (centroid) shifts are quoted relative to Fe metal standard at 300 K.

Figure 1 shows that at  $\sim 50$  GPa appreciable centralized intensity near zero velocity occurs. Evolution to higher pressure suggests that these are spectral components with collapsed internal magnetic fields (not plotted in the spectrum at 50 GPa, for the sake of clarity). This includes one with a comparatively

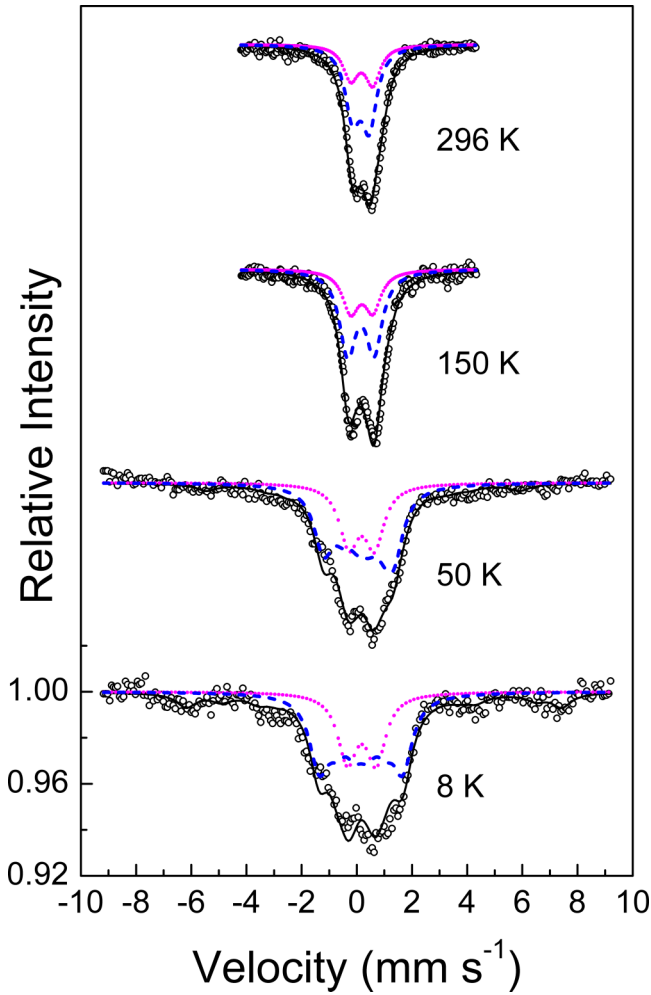


FIG. 2. Mössbauer spectra of CuFeO<sub>2</sub> at 95 GPa at variable cryogenic temperatures. Open circles are original experimental data. The solid line through experimental points is the overall theoretical fit. Dashed and dotted lines are subspectra corresponding to Fe<sup>3+</sup> and Fe<sup>2+</sup>, respectively.

small  $H_{hf}$  value in addition to a quadrupole doublet ( $H_{hf} = 0$ ). The abundances of these collapsed-field components increase with pressure. Abundances of these components constitute 80% of the total absorption area at the highest pressure reached in these experiments at 95 GPa, before failure of the anvils occurred at the next pressure increment.

The temperature evolution of the spectrum of this very-high-pressure phase at 95 GPa is shown in Fig. 2. Spectra at the lowest temperatures can be adequately fitted with two dominant components having  $H_{hf}$  values of 0 and  $\sim 10$  T, as well as minor remnant phase. The ratio of these two dominant 10 T and 0 T high-pressure spectral components is 2:1, respectively. The quadrupole doublet component ( $H_{hf} = 0$  T) has an isomer (centroid) shift value  $\delta_{IS} = 0.16$  mm s<sup>-1</sup> and quadrupole splitting  $\Delta_{QS} = 1.6$  mm s<sup>-1</sup> independent of temperature. The  $\Delta_{QS}$  parameter of the other component with  $H_{hf} = 10$  T has a distinctive temperature dependence.

The pressure dependence of the hyperfine interaction parameters of CuFeO<sub>2</sub> at room temperature are shown in Fig. 3. This conspicuously shows collapse of  $H_{hf}$  magnetic hyperfine

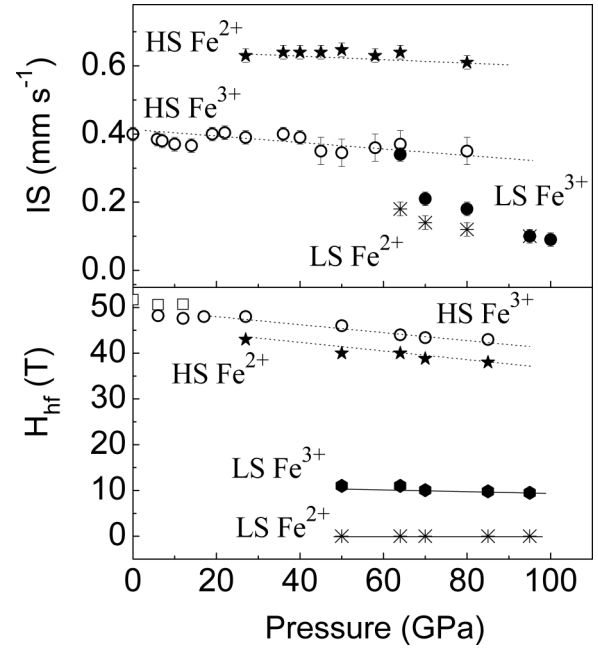


FIG. 3. Pressure dependence of hyperfine interaction parameters of CuFeO<sub>2</sub> at room temperature. Isomer shift values in top panel are quoted relative to Fe metal standard. Solid stars are values of high-spin Fe<sup>2+</sup>, open circles represent high-spin Fe<sup>3+</sup>, solid circles represent low-spin Fe<sup>3+</sup>, and asterisks (\*) are low-spin Fe<sup>2+</sup>. Squares are values of the four-sublattice phase near ambient pressure.

fields for emergent components beyond  $P \sim 50$  GPa. The change in  $\delta_{IS}$  values from distinctive Fe<sup>3+</sup> and Fe<sup>2+</sup> signatures at  $P < 50$  GPa, to lowered and similar values for both components needs to be emphasized. These changes are evidence of an evolution to different electronic states in the very-high-pressure phase of CuFeO<sub>2</sub>, onset at  $\sim 50$  GPa and hereafter designated as CuFeO<sub>2</sub>-VHP.

### B. Electrical resistance pressure evolution

CuFeO<sub>2</sub> is a wide band-gap semiconductor with a gap of  $E_g = 2.0$  eV at ambient pressure [13]. The pressure dependence of the CuFeO<sub>2</sub> resistance at 300 K is shown in Fig. 4. In the 10–27 GPa range the resistance  $R$  (300 K) decreases by more than three orders of magnitude, whereas  $\log_{10}[R(P)]$  has a much smaller change from 27 to 50 GPa. Above 50 GPa there is a much stronger pressure dependence of resistance where collapsed  $H_{hf}$  components emerge. The temperature dependence of the resistance at different pressures is also depicted in the inset of Fig. 4(a). The resistance has a negative temperature coefficient over the full temperature range up to the highest pressure of this study at 77 GPa, indicative of *nonmetallic* behavior and narrow-gapped semiconducting attributes throughout. Attempts to linearize the data in terms of Arrhenius, small polaron, and variable range hopping (VRH) models only exhibit this linearity in a restricted high-temperature range. This points to prevailing complex conductivity mechanisms likely involving both Cu and Fe species. Variable range hopping is applicable over a wider high-temperature range than the other models, especially in the majority CuFeO<sub>2</sub>-VHP phase at 77 GPa. This is associated

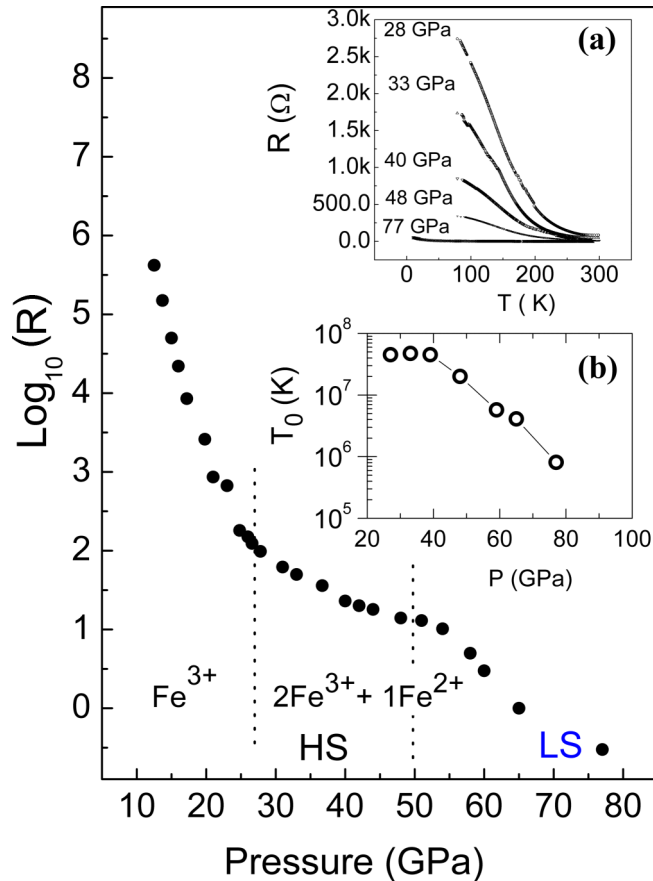


FIG. 4. Pressure dependence of  $\text{CuFeO}_2$  resistance measured at 300 K. Inset (a) shows temperature dependence of the resistance down to liquid helium temperatures. Inset (b) is the estimated Mott temperature  $T_0$  from fits to data in the high-temperature range 190–260 K using a variable range hopping model,  $\ln(R)$  versus  $1/T^{1/4}$ . Solid lines through points are to guide the eye.

with disorder due to a randomly varying potential from the  $\text{Fe}^{2+}$  and  $\text{Fe}^{3+}$  distributions in the lattice. Therefore we opt for an analysis in terms of VRH behavior,  $\ln(R)$  versus  $(1/T)^{1/4}$ . Estimates of the Mott (characteristic) temperature  $T_0$  and its pressure evolution are obtained from the gradients of linear regions of such plots [14,15]. Good linear fits to the data (not shown here), in a restricted range 190–260 K for most of the pressures and 140–300 K for the highest pressure, give the  $T_0$  pressure evolution in the inset of Fig. 4(b).  $T_0$  changes by two orders of magnitude in going from the  $\text{CuFeO}_2$ -HP2 phase,  $P < 50$  GPa, to the majority  $\text{CuFeO}_2$ -VHP phase at  $P > 77$  GPa. It is still appreciable in the majority  $\text{CuFeO}_2$ -VHP phase at 77 GPa and by a simplified linear extrapolation of the data in Fig. 4(b)  $T_0$  reaches  $\sim 10^5$  K at 100 GPa. The estimate of  $T_0$  in the range 50–77 GPa is an “effective Mott temperature” of the original mixed-valence  $\text{CuFeO}_2$ -HP2 state coexisting with the emergent  $\text{CuFeO}_2$ -VHP phase. For comparison, Arrhenius or small polaron fits of linearized data in restricted high-temperature ranges (200–250 K) give activation energy estimates of 0.1 eV for the  $\text{CuFeO}_2$ -HP2 phase at  $P < 50$  GPa and  $\sim 0.05$  eV in the majority phase at 77 GPa.

#### IV. DISCUSSION AND CONCLUDING REMARKS

Figure 3 emphasizes that the evolved components at  $P > 50$  GPa have collapsed  $H_{hf}$  values. Moreover there is a change in  $\delta_{IS}$  values typical of  $\text{Fe}^{3+}$  ( $\delta_{IS} \sim 0.4 \text{ mm s}^{-1}$ ) and  $\text{Fe}^{2+}$  ( $\delta_{IS} \sim 0.62 \text{ mm s}^{-1}$ ) for the high-spin states, to near coincident lower values of  $\delta_{IS} < 0.2 \text{ mm s}^{-1}$ . Such changes would be anticipated for a high-spin (HS)  $\rightarrow$  low-spin (LS) electronic modification [11]. This occurs concurrently for both valences, signifying that this is a long-range cooperative phenomenon.

This is a result of the breakdown of Hund’s rule at very high density. Assuming octahedral coordination of Fe, reducing interatomic spacings results in an increase in the crystal field splitting of  $3d$  electronic levels. There is a corresponding increased cost of occupying higher-lying  $e_g$  electronic states, which are originally separated from lower-lying  $t_{2g}$  orbital levels by the crystal field splitting designated  $\Delta = 10Dq$  ( $\sim 1$  eV). At a critical pressure this increased cost will supersede the energy gain from maximizing the possible pairs of parallel spins in different  $3d$  orbitals on the same site (Hund’s rule, whereby there is effectively a gain of  $-J \sim -1$  eV for each set of parallel spins, from intratomic “on-site” ferromagnetic exchange coupling). When  $\Delta > 3J$  for  $3d^5$  ( $\text{Fe}^{3+}$ ) and  $3d^6$  ( $\text{Fe}^{2+}$ ) electronic configurations, antiparallel spin pairing in lower-lying ( $t_{2g}$ ) electronic orbital states becomes energetically favorable and HS  $\rightarrow$  LS crossover ensues [16].

In  $\text{Fe}^{3+}$  compounds the  $3d^5$  electronic configuration of the HS state has maximally unpaired electron spins,  $(\uparrow\uparrow\uparrow)(\uparrow\uparrow)$ , distributed in  $t_{2g}$  and  $e_g$  orbitals as  $(t_{2g})^3(e_g)^2$  and the LS configuration, spin paired  $(\uparrow\downarrow\uparrow\downarrow\uparrow)$ , has  $(t_{2g})^5(e_g)^0$  occupation. In the LS state the total spin moment is from the  $S = 1/2$  net atomic spin. Magnetic (interatomic) coupling is expected to be much weaker than in the HS  $S = 5/2$  configuration.

In the  $\text{Fe}^{3+}$  HS state,  $H_{hf}$  for iron oxides is typically  $\sim 50$  T, arising primarily from the Fermi contact contribution [17]. In  $\text{CuFeO}_2$ -VHP long-range magnetic ordering with  $H_{hf} \sim 10$  T for one of the subspectra (see Figs. 2 and 3) is compatible with an  $\text{Fe}^{3+}$  LS scenario. The  $H_{hf}$  change of 50 T  $\rightarrow$  10 T corresponds to  $5/2 \rightarrow 1/2$  atomic spin crossover, in Fig. 3. This is corroborated by a temperature-dependent  $\Delta_{QS}$  for this subspectrum as a result of the thermal Boltzmann distribution of the “hole” in  $t_{2g}$  levels corresponding to  $(t_{2g})^5$  orbital occupancy [11]. All these characteristics are compelling evidence for an  $\text{Fe}^{3+}$  LS state in  $\text{CuFeO}_2$ -VHP. There is an unusually high onset temperature of static magnetic ordering of this spin-paired (low moment) state,  $T_M \sim 50$  K at 95 GPa, see Fig. 2. For such a comparatively Fe-dilute oxide, this must be attributable to the reduced interatomic spacings at such high densities. The increased orbital overlap and compacted structural configuration is such that magnetic coupling is enhanced appreciably, despite a large reduction in spin-derived magnetic moment from  $5/2 \rightarrow 1/2$   $3d$  spin crossover.

The other spectral component of  $\text{CuFeO}_2$ -VHP exhibits no magnetic hyperfine splitting down to 5 K and  $\Delta_{QS}$  of this doublet is independent of temperature, Fig. 2. These are signatures of the fully spin-paired ( $S = 0$ )  $\text{Fe}^{2+}$  LS state  $(\uparrow\downarrow\uparrow\downarrow\uparrow\downarrow)$ , with  $(t_{2g})^6$  orbital occupancy. Its lower-pressure HS counterpart ( $S = 2$ ) in  $\text{CuFeO}_2$ -HP2 has  $(t_{2g})^4(e_g)^2$ , with

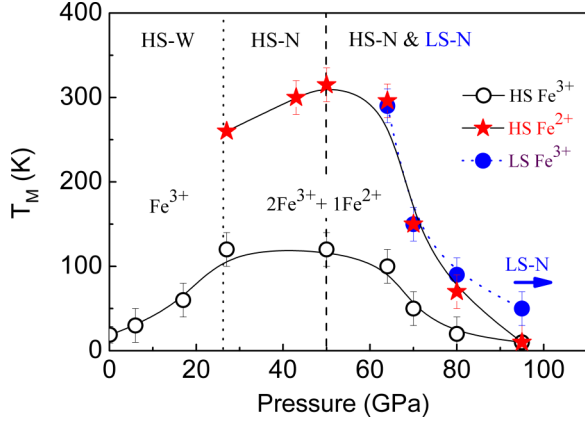


FIG. 5. Magnetic-electronic  $P$ - $T$  phase diagram of CuFeO<sub>2</sub>.  $T_M$  is the magnetic ordering temperature. HS-W and HS-N designate the high-spin wide- and narrow-gap semiconducting regimes, respectively. LS-N is the low-spin narrow-gap semiconducting phase. Solid lines through points are to guide the eye.

spin depiction ( $\uparrow\downarrow\uparrow\uparrow$ )( $\uparrow\uparrow$ ). The  $\delta_{IS}$  of the LS Fe<sup>2+</sup> component nearly coincides with that of the magnetic Fe<sup>3+</sup> LS component in Fig. 3, consistent with numerous cases of spin-crossover compounds at ambient pressure [11].

Also recall the pressure dependence of resistance at 300 K in Fig. 4. An appreciable change in pressure dependence occurs at  $\sim 50$  GPa. This coincides with the emergence of collapsed  $H_{hf}$  components of CuFeO<sub>2</sub>-VHP. This also serves to delineate  $P \sim 50$  GPa as an (electronic) phase transition boundary.

These results permit us to construct a magnetic-electronic  $P$ - $T$  phase diagram for CuFeO<sub>2</sub> up to  $\sim 100$  GPa as depicted in Fig. 5. Xu *et al.* [2] have already rationalized that in mixed-valence HS CuFeO<sub>2</sub>-HP2 the Cu<sup>1+</sup>  $\rightarrow$  Fe<sup>3+</sup> electronic charge transfer leads to Cu<sub>( $S=1/2$ )</sub><sup>2+</sup>/Fe<sub>( $S=2$ )</sub><sup>2+</sup> and Cu<sub>( $S=0$ )</sub><sup>1+</sup>/Fe<sub>( $S=5/2$ )</sub><sup>3+</sup> in the superexchange pathways, which account for the high  $T_M$  values of Fe<sup>2+</sup> compared with Fe<sup>3+</sup>. At  $P > 50$  GPa decreasing amounts of this species continue to account for high  $T_M$  values. As pressure rises  $T_M$  decreases monotonically as regions of low-moment Fe<sup>3+</sup> ( $S = 1/2$ ) and Fe<sup>2+</sup> ( $S = 0$ ) nucleate with ever increasing abundance and impact on the superexchange pathways, until domination at  $P > 77$  GPa. Moreover it appears that this high-density LS state remains nonmetallic as manifested in persistent narrow-gap semiconducting behavior and a relatively high Mott temperature  $T_0$  of  $10^6$ – $10^5$  K in the range 80–100 GPa; see Fig. 4(b). Based on this  $T_0$  range in the LS state, the average hopping distance  $R$  has increased by a factor of (only) 1.5–2 compared to that of the HS state at  $P < 50$  GPa. For this purpose we have used the well known VRH formulations for  $k_B T_0 \sim \alpha^3/N_F$  and  $R \sim [\alpha N_F k_B T]^{-1/4}$ , where  $\alpha^{-1}$  is the localization length  $\xi$  giving the approximate extent of the localized charge carrier wave packet [14,15]. It has also been assumed that the density of states at the Fermi level  $N_F$  has not altered radically at HS/LS crossover. These estimates hint at charge carrier localization being persistent up to at least 100 GPa in the LS state, if there is no drastic structural transition to radically change the electronic band structure.

We now propose an explanation as to how a nonmetallic LS state becomes stabilized at very high pressures in CuFeO<sub>2</sub>-

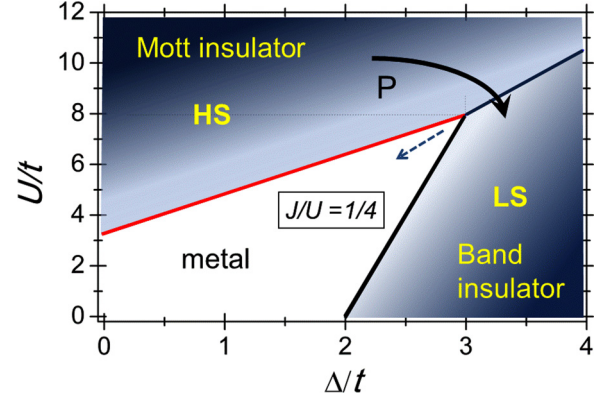


FIG. 6. Conceptual phase diagram of the two-band model, to illustrate electronic ground-state dependency on relative values of  $U/t$ ,  $\Delta/t$ , and  $J$  parameters for  $J/U = 1/4$ . The size of the charge (conductivity) gap is indicated by color intensity (white=no gap). Adapted from Refs. [18,19]. The dashed arrow indicates how the triple point would move for decreasing  $J/U$  values. The black arrow is an indication of the trajectory followed by CuFeO<sub>2</sub> under pressure, in a proposed similar phase diagram of a mixed-valence compound involving a five-band model.

VHP. This is based on a phase diagram involving  $U/t$  versus  $\Delta/t$  electronic parameters, where the hopping integral  $t$  is related to  $3d$  bandwidth. In the last decade such a phase diagram has been developed for various  $J/U$  ratios to consider the impact of Hund's coupling  $J$  in multiorbital Hubbard models; see Fig. 6. This is specifically for a two-band system with two electrons (half filling) [18,19], but is considered to have wider applicability in multiorbital systems. A strong pressure dependence of crystal field  $\Delta$  compared with  $t$  leads to a corresponding appreciable increase in the ratio  $\Delta/t$  compared with the decrease in  $U/t$  ratio [20]. This has the possibility to take the system across an HS/LS phase boundary to concurrent large  $U/t$  and  $\Delta/t$  regions of the phase diagram, to where a narrow charge-gapped (nonmetallic) LS phase is stabilized. This pressure-evolved trajectory is depicted in the conceptual phase diagram of Fig. 6, whereas a trajectory to a metallic phase (Mott transition) would occur, for example, if  $U/t$  were to have a comparable pressure dependence on  $\Delta/t$ . This is also dependent on where in the phase diagram the system is initially located at ambient or low pressures. The work of Kuneš *et al.* [18,19], and references therein, to obtain Fig. 6 is for a single valence species in the lattice.

We contend that a similar representation of Fig. 6 may be applicable to the HS  $\rightarrow$  LS transition of Figs. 3–5 in CuFeO<sub>2</sub>-VHP. This involves a five-band system (nondegenerate  $e_g$  and  $t_{2g}$  bands) with mixed valences from  $3d^5$  and  $3d^6$  states distributed over the lattice sites (in the ratio 2:1). The pressure response of CuFeO<sub>2</sub>-HP2 as a starting point is such that the ratio  $U/t$  remains comparatively high as  $t$  changes under pressure, but the increasing  $\Delta/t$  has a much stronger pressure dependence. Thus compressing CuFeO<sub>2</sub> to a megabar takes the system into the large  $U/t$  and  $\Delta/t$  regions of the  $(U/t, \Delta/t, J/U)$  electronic phase diagram. This transits it across an HS/LS phase boundary into the narrow charge-gapped LS state where strong correlations are persistent,  $U/t \gg 1$ , in analogy to the depiction in Fig. 6.

In conclusion, CuFeO<sub>2</sub>-VHP at a megabar has been shown to stabilize as a mixed-valence Fe 3*d* spin-paired magnetic narrow-gapped semiconducting compound. This has an unusually high magnetic ordering temperature of ~50 K, given the presence of Fe 3*d* spin-paired species and associated nearly fully quenched atomic spin moments in the lattice. Moreover the nonmetallic behavior of this partially filled 3*d* band system is suggestive of persistent strong electron correlations. To date these combined features are normally found in magnetic *high-spin* mixed-valence semiconducting metal oxide analogs [21]. Hund's rule is abolished in CuFeO<sub>2</sub>-VHP because of restricted atomic volumes at these high densities, particularly for the

high-spin Fe<sup>2+</sup> species. A welcome complement to this study would be for XRD structural studies to be effected, to gauge the interplay between lattice response and the posited electron spin-pairing transition.

#### ACKNOWLEDGMENTS

This work was supported by ISF (Israel) Grant No. 1189/16. We further acknowledge discussions on the content of this work with members of the TAU high-pressure physics group.

- 
- [1] W. M. Xu, M. P. Pasternak, and R. D. Taylor, *Phys. Rev. B* **69**, 052401 (2004).
- [2] W. M. Xu, G. K. Rozenberg, M. P. Pasternak, M. Kertzer, A. Kurnosov, L. S. Dubrovinsky, S. Pascarelli, M. Munoz, M. Vaccari, M. Hanfland *et al.*, *Phys. Rev. B* **81**, 104110 (2010).
- [3] N. Terada, T. Osakabe, and H. Kitazawa, *Phys. Rev. B* **83**, 020403 (2011).
- [4] N. Terada, D. D. Khalyavin, P. Manuel, T. Osakabe, P. G. Radaelli, and H. Kitazawa, *Phys. Rev. B* **89**, 220403(R) (2014).
- [5] T. R. Zhao, M. Hasegawa, H. Takei, T. Kondo, and T. Yagi, *Jpn. J. Appl. Phys.* **35**, 3535 (1996).
- [6] A. Pabst, *Am. Mineral.* **31**, 539 (1946).
- [7] S. Mitsuda, H. Yoshizawa, N. Yaguchi, and M. Mekata, *J. Phys. Soc. Jpn.* **60**, 1885 (1991).
- [8] G. Y. Machavariani, M. P. Pasternak, G. R. Hearne, and G. K. Rozenberg, *Rev. Sci. Instrum.* **69**, 1423 (1998).
- [9] G. R. Hearne, M. P. Pasternak, and R. D. Taylor, *Rev. Sci. Instrum.* **65**, 3787 (1994).
- [10] The hyperfine interaction parameters including Fe site abundances are derived from fitting the spectral envelope with Lorentzian subcomponents. The isomer (chemical) shift  $\delta_{IS}$  is proportional to the *s*-electron density at the Fe nucleus and is influenced by *d*-electron shielding. The quadrupole doublet splitting or line shift,  $\Delta_{QS}$ , is proportional to the deviation from cubic symmetry of both the surrounding electron configuration and nearest-neighbor atoms. The  $\delta_{IS}$ ,  $\Delta_{QS}$ , and  $H_{hf}$  (from magnetically split hyperfine structure) parameters have distinct "fingerprint" values for both valences and spin states of Fe<sup>2+</sup>(3*d*<sup>6</sup>) and Fe<sup>3+</sup>(3*d*<sup>5</sup>). In complex spectra, with appreciable overlap of subcomponents, mainly  $\delta_{IS}$  and to a lesser extent  $H_{hf}$  values of fitted subspectra are obtained with good reliability, to establish the electronic state of the Fe.
- [11] P. Gütllich, E. Bill, and A. X. Trautwein, *Mössbauer Spectroscopy and Transition Metal Chemistry: Fundamentals and Applications* (Springer, Berlin, 2011).
- [12] The quadrupole splitting  $\Delta_{QS}$  is half the value of the quadrupole coupling  $e^2q_{zz}Q$  for a diamagnetic or paramagnetic Fe phase manifested as a spectral doublet.
- [13] V. R. Galakhov, A. I. Poteryaev, E. Z. Kurmaev, V. I. Anisimov, S. Bartkowski, M. Neumann, Z. W. Lu, B. M. Klein, and T.-R. Zhao, *Phys. Rev. B* **56**, 4584 (1997).
- [14] N. F. Mott, *Metal-Insulator Transitions*, 2nd ed. (Taylor and Francis, London, New York, 1990).
- [15] M. Viret, L. Ranno, and J. M. D. Coey, *Phys. Rev. B* **55**, 8067 (1997).
- [16] S. G. Ovchinnikov, *J. Exp. Theor. Phys.* **107**, 140 (2008).
- [17] The magnetic hyperfine field is a result of the nuclear Zeeman splitting of <sup>57</sup>Fe nuclear levels due to an internal magnetic field at the nucleus. The primary contribution to this internal field,  $H_{hf}$ , is from the contact term. This is the effect of *d*-electron spin polarization on the *s* electrons. Other contributions to  $H_{hf}$  are from comparatively small dipolar and orbital terms. In HS ferric iron the orbital and dipolar terms are negligibly small. The orbital term in HS ferrous iron and LS ferric iron may be appreciable and of opposite sign to the contact term. At well below the magnetic ordering temperatures,  $H_{hf}$  in HS ferric oxides is typically clustered around ~50 T whereas in ferrous compounds it may range from near zero to 44 T depending on the orbital configuration.
- [18] J. Kuneš, I. Leonov, M. Kollar, K. Byczuk, V. I. Anisimov, and D. Vollhardt, *Eur. Phys. J.: Spec. Top.* **180**, 5 (2010).
- [19] J. Kuneš and V. Křápek, *Phys. Rev. Lett.* **106**, 256401 (2011).
- [20] It is primarily the crystal field splitting  $\Delta$  and hopping (overlap) integral *t* related to 3*d* bandwidth which are dependent on *intersite* spacing (i.e., pressure). *On-site* electronic parameters, Coulomb repulsion *U*, and Hund's coupling *J* are expected to have a comparatively much weaker pressure dependence, if any.
- [21] P. A. Cox, *Transition Metal Oxides: An Introduction to Their Electronic Structure and Properties* (Clarendon Press, Oxford, UK, 1995).